Supplementary Information

1.1 Calculation of scaling parameter and cell size

At 37°C in LB media, an estimated cell length (including end-caps) would be 2.482 μm while the diameter would be 0.933 μm [1].
Let the order of the HiC contact frequency matrix be N, length of the cell (including end caps) be L, diameter be d and size of each polymer bead be σ (see Figure S1).
Therefore, the number of beads in the polymer = N
Let l = L - d, r = $\frac{d}{2}$
Therefore, volume of the cell = $\frac{4}{3}\pi r^3 + \pi r^2 l = \pi r^2(\frac{4}{3}r + l)$
Assuming a volume fraction f_r,

$$\text{the volume occupied by the DNA} = f_r \text{ x Volume of the cell} = \pi r^2 f_r(\frac{4}{3}r + l) \quad \text{(S1)}$$

$$\text{But the volume occupied by the DNA} = \frac{4}{3}\pi(\frac{\sigma}{2})^3 = \frac{\pi\sigma^3}{6} \quad \text{(S1)}$$

On comparing equations (S1) and (S1), we get

$$\sigma = \sqrt[3]{\frac{6f_r r^2}{N}(\frac{4}{3}r + l)} \quad \text{(S1)}$$

Using $f_r = 0.1$[2] and the cell dimensions stated above for a resolution of 5 kbp (N=928), $\sigma = 0.067348$ μm.
Upon setting $\sigma = 1$ and scaling the cell dimensions provided above, we get the cell length (including end-caps) equals to 36.884 and the diameter equals to 13.864 in reduced (simulation) units.

1.2 Calculation of the number of beads present in replication forks

Since we know from the G value how much DNA one cell has, and that the replication proceeds almost with equal speeds bidirectionally from oriC[3], we defined and calculated a parameter f which shall provide us the fraction of DNA replicated. The usefulness and calculation of f will become clear in the forthcoming details. Let there be a two forked system as depicted by Figure S2.

Therefore, the amount of DNA present is $(1-f) + f + f + 2f^2$ which is equal to $G\times$ the amount of DNA contained by one chromosome.
For our system with a resolution of 5 kbp, there are 928 (4.64Mbp/5kbp) beads that represents the amount of DNA contained by one chromosome.
Therefore,
Unreplicated DNA = $(1-f)$
DNA per primary fork = $f(1-f)$
DNA per secondary fork = f^2
Therefore, $2f^2 + 2f + 1 = G$

or, $2f^2 + 2f + (1 - G) = 0$
Upon solving the above equation and using the condition that f>0, we get

$$f = \frac{-1 + \sqrt{8G - 7}}{4} \tag{S1}$$

For two chromosomes with a total G=3.6, we assume that each chromosome will have a G=1.8. Thus, for G=1.8, we have $f = 0.43$. Using this value of f, we get 529 unreplicated beads, 456 beads in primary forks and 687 beads in secondary forks. Thus a total of 1672 beads per chromosome and a 3344 beads per cell.

1.3 Interaction potenitals

1.3.1 The cell boundary

The cell boundary has been implemented by using a restraining potential of the form

$$V_{res}(r; R_0) = \frac{1}{2} k_{res} |\vec{r} - \vec{R_0}|^2 \ \mathbf{H}(|\vec{r} - \vec{R_0}|) \tag{S1}$$

H is a step function and activates if a particle goes out of the confinement, which, here is a spherocylinder. R_0 is the center of the spherocylinder. k_{res} determines how rigid is the cell wall. For simulations we have used 310 kJ mol$^{-1}\sigma^2$, slightly higher than k_{adj}, making it the highest in magnitude among all the force constants present.

1.3.2 Non-bonded interactions

Since no information is known about the attractive interactions between DNA beads at 5 kbp resolution, we assume that all the attractive interactions bringing regions of the DNA close to each other have been captured by HiC. Therefore the non-bonded interactions are purely repulsive and are given by

$$V_{nb}(r) = \frac{A}{r^{12}} \tag{S1}$$

where A = $4\epsilon\sigma^{12}$. Equation (6) is simply the repulsive part of the Lennard-Jones potential. This also ensures that polymer beads do not overlap significantly when equilibration is performed. For the simulations, A=1.0 has been used.

1.3.3 Finding a good transfer function

The main purpose of the current work is to develop a quantitative model that can explore the higher order organisation of the 4.64 Mbp long, *E. coli* chromosome. Towards the end, following the protocol outlined in Figure 1 and explained in *Methods*, we integrate recently reported Hi-C interaction matrix of *E. coli* chromosome [4] within a polymer based beads-on-a-spring model. The chromosome, thereby modelled, is subsequently

subjected to a langevin dynamics simulation at a friction coefficient of 1 $\sqrt{\frac{m\epsilon}{\sigma}}$ and temperature of 303K. The simulation observables are statistically averaged over the last 2000 frames from the 200 trajectories.

In previous attempts to model the chromosome using Hi-C data[4, 5], a variant of the inverse function has been used to convert contact probabilities to distances(S1).

$$D \propto P^{-s} \tag{S1}$$

where D is the distance matrix and P is the contact probability matrix. The operation is elementwise inverse of matrix elements of P raised to a power s. s can be obtained by comparing the distances obtained by varying s to an experimentally obtained set of distances[4]. We have used $s = 1.0$ for our studies[5] with a proportionality constant of σ which is the bead size. Thus when the contact probability is 1, the distance of a Hi-C bond is σ. An earlier approach to model the bacterial chromosome using Hi-C data involved a low, but constant, force constants for all the contacts that are put into the model[6]. Here we scaled the force constants with respect to the distances, which in turn makes the force constants scale with contact probabilities. We hypothesize that if a pair of chromosome regions have a high contact probability between them, then they have been actively brought together and appear as a 'contact' in most cells when Hi-C is performed. Whereas regions with low contact probabilities are a result of the random collisions between different regions of the chromosome. To mimic this stochastic behaviour, we used a function, which we call the "transfer function", that would scale in such a way so that the lower the contact probability, lower is the force constant between two such regions. Thus for regions with no contact, there would not be any restraint or a restraint with a relatively very weak force constant, thereby introducing random fluctuations in their equlibrium distances.

First we tried a simple inverse transfer function as shown in Eq. (S1). k_0 is a parameter and does not effect the chromosome organization in anyway. It controls the maximum strength of the "Hi-C" bonds between two beads, thus can be chosen to arbitrarily low with respect to the adjacent beads' bond strength. For all simulations, $k_0 = 10$ was used.

$$k_{ij} = \frac{k_0}{D_{ij}} \tag{S1}$$

Though the distances we obtained correlated well with existing experimental data (Figure S5), but the chromosome was found to be very condensed inside the cell (Figure S4a), which is not in agreement with the linear density profiles of the chromosome from experiments and theoretical studies[7, 8]. Not to mention that it is difficult to deal with very low probabilities which get converted to very large distances. We had to define a distance cutoff (diameter of the cell), beyond which we did not consider them as contacts anymore. But the choice was arbitrary.

After using a simple inverse function, we tried a gaussian function to get the force constants (Eq. (S1)). The gaussian ensured that the at infinites and large distances, the force constant scaled down to such a low value that it can be safely ignored. Also, only a small fraction of the total number of contacts were actually used when we used Eq. (S1) for simulations as can be seen from Figure S4b and Figure S6. We see that

when we use the gaussian, the important regions of contacts are mainly located along the diagonal and the small patch on the ends of the off-diagonal due to circularity of the chromosome. We see that such a small number of contacts is able to predict the whole contact parobbaility matrix with a high accuracy (Figure S4c). We also see that predictions are better when we used Eq. (S1). The gaussian also lets the chromosme spread out into the cell volume much more than the inverse transfer function (Figure S4d). This is a more realistic image as seen from previous theoretical and experimantal studies[7, 8]. Thus we believe that Eq. (S1) is a much better transfer function to generate more plausible 3D conformations.

1.3.4 Bonded interactions

Adjacent beads of the polymer are connected by strong (300 kJ $\text{mol}^{-1}\sigma^2$) harmonic springs with σ as the equilibrium bond length. This has been implemented by introducing harmonic force fields between adjacent beads. HiC contacts have also been modelled as harmonic springs but with variable strengths and variable bond lengths.
Let the HiC contact probability matrix be P and a distance matrix, D, has been defined such that

$$D_{ij} = \frac{\sigma}{P_{ij}} \tag{S1}$$

where ij suggests the element in the i^{th} row and j^{th} column of the matrices. It should be noted that the matrix P is a sparse matrix. Therefore a lot of the elements in D would be ∞. They would be taken care by the model itself as discussed below. The force constants for the bonds incorporating the HiC contacts into the model is given by

$$k_{ij} = k_0 e^{-\frac{(D_{ij}-\sigma)^2}{w}} \tag{S1}$$

As per Hooke's law,

$$\begin{aligned} V_{HiC}(D_{ij}) = &\ \frac{1}{2}k_{ij}(D_{ij} - r_{ij})^2 \\ \implies \quad V_{HiC}(D_{ij}) = &\ \frac{1}{2}k_0 e^{-\frac{(D_{ij}-\sigma)^2}{w}}(D_{ij} - r_{ij})^2 \end{aligned}$$

For $D_{ij} = \infty$, $V_{HiC}(D_{ij}) = 0$.

In equation (5), k_0 and w are parameters that need to be optimised but k_0 is just a amplitude term that determines the upper limit to the force constants of the "HiC bonds". Since a high force constant makes bonds rigid, a very high value of k_0 will only effect the net dynamics of the polymer. k_0 does not in any form effect the equilibrium distances of the HiC bonds, thus has negligible effect on the overall polymer configuration. For all our simulations we used $k_0 = 10$. This choice is somewhat arbitrary, but the value of k_0 is low when compared to the force constant of the backbone bonds. This is not arbitrary. The reason for such a choice is that we have used contact **probability** to model these bonds. Therefore, a non-zero number of times it should be seen that there

exists no HiC-contact between beads i and$j$ if we sample from a large set of time series distances at equilibrium between i and j. A low force constant would lead to larger deviations in the distance between the two beads during simulations and should mimic the sampling, i.e. if we look at the probability distribution of the time series distance data of the HiC bond length between two beads i and j, we shall see that the equilibrium would have a probability almost equal to P_{ij}.
w needs to be optimized for each unique HiC contact probability matrix. It determines the width of the Gaussian in equation (5), therefore behaves as a filtering parameter. For example, from Figure S7 it can be seen that for a higher value of w, more number of k_{ij} have magnitudes greater than 0. This incorporates more HiC bonds into the system. To speed up simulations, we did not consider bonds whose force constants were lower than 10^{-7}. Such bonds are very weak and do not effect the conformation(s) of the chromosome significantly.

1.4 Optimization of w

The metric used to optimize w is a Pearson correlation between the experimental and the *filtered* simulated contact probability matrices. Many elements in the contact probability matrix are zero due experimental limitations and experimental protocol. But in the simulated HiC matrix, we do not have any zero, but a base value of contact probability(since no two bead can go beyond L). Thus to make them comparable we set those values to zero the simulated matrix which are also zero in the experimental matrix. This is what we refer to when we mention filtered/filtering. Then the matrices are "flattened" in the sense that the 2D sparse matrix is converted to a 1D array with no non-zero elements. The zeros are removed so as to get the Pearson correlation between the non-zero elements only. Considering the zeros after filtering would have contributed to a higher value of the correlation coefficient, thereby reducing its sensitivity to w. In this way we are able to perform an element wise comparison between the matrices. Table S1 provides the optimization table.

1.5 Generation of simulated contact probability matrix

Using the last 2000 frames of k-th simulation, we generate a distance matrix D^k whose distances have been averaged over the number of frames. To generate a matrix with similar dimensions as that of the Hi-C contact probability matrix, for each frame we use the average distances for bead pairs that have been replicated. We also made sure not to consider distances between beads from different forks. We generate the final simulated distance matrix D_{sim} by averaging over those matrices.

$$D_{\text{sim}} = \frac{1}{n}\sum_{k=1}^{n} D^k \tag{S1}$$

Similarly, we also generate P^k which is the simulated contact probability matrix for the k-th simulation.

$$P_{ij}^k = \frac{\sigma}{D_{ij}^k} \tag{S1}$$

The simulated probability matrix P_{sim} is an average over P^k.

$$P_{\text{sim}} = \frac{1}{n}\sum_{k=1}^{n} P^k \tag{S1}$$

We have used n=200, i.e. we have used 200 simulations for the averaging.
It should be noted that $P_{\text{sim}} \neq \frac{\sigma}{D_{\text{sim}}}$, and it is evident from the definitions of $P^k, D^k, P_{\text{sim}}, D_{\text{sim}}$ given by equations (7) - (9).
Each frame corresponds to a microstate of the ensemble of chromatin conformations whose average is the experimental HiC matrix. Since a set of 2000 frames belong to a particular initial conformation, instead of generating 200 x 2000 = 4 x 10^5 matrices and performing an average over them, we average over 200 matrices, which have been averaged frame-wise. We also generate a distance matrix averaged over frames and simulations. This matrix is used for all distance related calculations or analysis.

1.6 Filtering of simulated contact probability matrices

A lot of rows and columns in the experimental contact probability matrix are zero. This can be due to two reasons: i) there is no contact between those two regions. ii) the region is too compact for Hi-C to detect any contact. Since they are zero, after incorporating into the model, "collisions" between such regions are purely random, even though they might be highly dense. This can lead to wrong interpretation of the data. To avoid this, we filter the simulated contact probability matrix by replacing elements in the matrix with zeros which are also zero in the experimental matrix. Thus we cannot get more information than what the experimental holds, but misinterpretations can be avoided. Solely for the purpose of having a better contrast within a matrix, we have raised each element to a power of 0.55 , only during plotting, so as to enhance the smaller values. For all numerical analysis we have used non-enhanced matrices.

1.7 Comparison between matrices

To compare matrices, we first *flatten* the matrices. Flattening simply means we convert the matrix into an 1D array, where each consecutive row adds to the array after the previous row. This array would thus be n x n long for a contact probability matrix of order n. Since the values which are zero in the experimental matrix are already zero, we recreate an array without any zeros. Two such arrays, without any zeros are compared for correlation or linear fitting. For absolute difference analysis also, we do not consider the zeros.

1.8 Generation of initial structures

Our initial conformations for the different G values we simulated are given in Figure S3. For each G, their respective initial configuration was first energy minimized with the confinement and the Hi-C interactions to make the conformations overlap-free and

to confine them properly. With the energy minimized conformation, MD simulations for 2×10^6 steps were performed. The final conformation obtained from MD was then subjected to stochastic dynamics at 310.15 K for 2×10^6 steps. 200 conformations from the last 1000 steps were extracted at equal intervals which served as initial conformations for the production runs.

1.9 Units

We have used a conversion similar to what Liu et al have used [9]. Below, reduced units and their conversion to real units have been summarized.

Quantity	**Symbol**	**Reduced Units**	**Real Units**
Length	σ	1	50.286 nm
Mass	m_0	1	325×10^4 amu
Time	t_{red}	1	1 ms
Temperature	T	1	1K

1.10 Rendering 3D conformations

We have used the open-source package Visual Molecular Dynamics (VMD)[10] to render the representative 3D conformations of the chromosome model.

2 Supplementary Tables

Table S1: Optimization table

w	R
0.10	0.852
0.15	0.859
0.20	0.865
0.25	0.867
0.30	0.868
0.35	0.867
0.40	0.866

Table S2: Average radius of gyration (R_g) of all macrodomains, non-structured regions in μm.

MD	G=3.6	G=1.8	G=1.0
Ori	0.267± 0.015	0.259±0.012	0.239± 0.022
NSR	0.179± 0.014	0.171±0.010	0.176± 0.014
Right	0.200± 0.021	0.192±0.017	0.225± 0.021
Ter	0.234± 0.029	0.243±0.028	0.336± 0.025
Left	0.192± 0.012	0.180±0.009	0.187± 0.011
NSL	0.197± 0.014	0.194±0.010	0.202± 0.016

Table S3: Macrodomain overlap scores

MD1	MD2	G=3.6	G=1.8	G=1.0	control(G=3.6)
NS-R	Right	0.251±0.048	0.157±0.030	0.134±0.024	0.428±0.052
NS-R	Ter	0.210±0.0.42	0.119±0.026	0.206±0.045	0.359±0.054
NS-R	Left	0.075±0.0.42	0.100±0.017	0.216±0.031	0.349±0.069
NS-R	NS-L	0.075±0.036	0.120±0.023	0.166±0.042	0.447±0.061
NS-R	Ori	0.304±0.029	0.124±0.009	0.343±0.080	0.504±0.045
Right	Ter	0.435±0.055	0.468±0.063	0.337±0.035	0.587±0.055
Right	Left	0.130±0.059	0.081±0.036	0.001±0.002	0.461±0.064
Right	NS-L	0.154±0.051	0.084±0.028	0.025±0.015	0.413±0.057
Right	Ori	0.216±0.040	0.119±0.017	0.218±0.049	0.494±0.044
Ter	Left	0.337±0.056	0.229±0.033	0.162±0.036	0.511±0.058
Ter	NS-L	0.163±0.046	0.081±0.025	0.199±0.037	0.371±0.056
Ter	Ori	0.223±0.039	0.296±0.034	0.253±0.049	0.459±0.045
Left	NS-L	0.331±0.046	0.296±0.034	0.320±0.047	0.478±0.072
Left	Ori	0.149±0.030	0.078 ±0.011	0.095±0.038	0.518±0.058
NS-L	Ori	0.233±0.030	0.123±0.010	0.233±0.033	0.638±0.035

3 Supplementary Figures

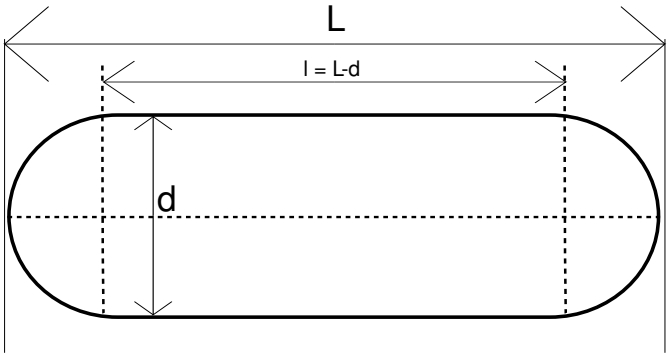

Figure S1: Cell dimensions

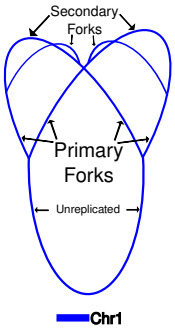

Figure S2: Schematic of a replication fork

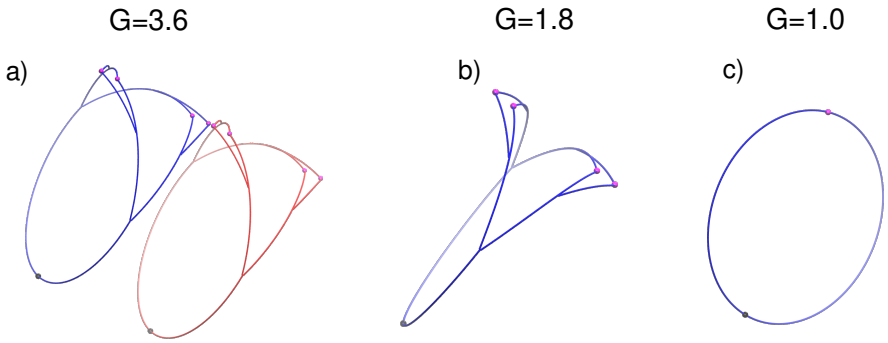

Figure S3: **a)** Starting conformation for G=3.6. **b)** Starting conformation for G=1.8. **c)** Starting conformation for G=1.0. OriCs have been coloured in magenta while difs have been coloured in black.

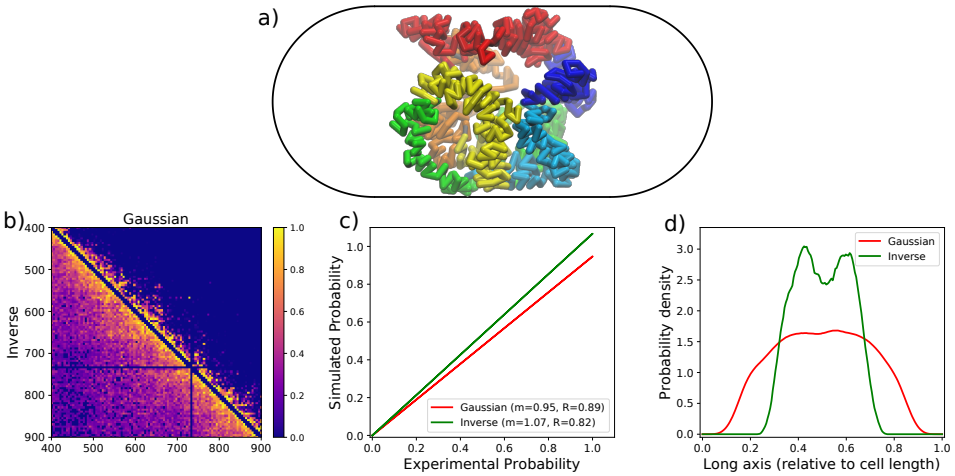

Figure S4: a) A snapshot of the 3D conformation for simulations using Eq. (S1). **b)** Comparison between the force constant matrices for Eqs. (**1**) and (S1). The lower half of the plot is for Eq. (S1) while the upper half is for Eq. (**1**). **c)** Compairson of the Hi-C simulated matrices using Eqs. (**1**) and (S1). **d)** Linear density along the long axis of the cell for simulations using Eqs. (**1**) and (S1).

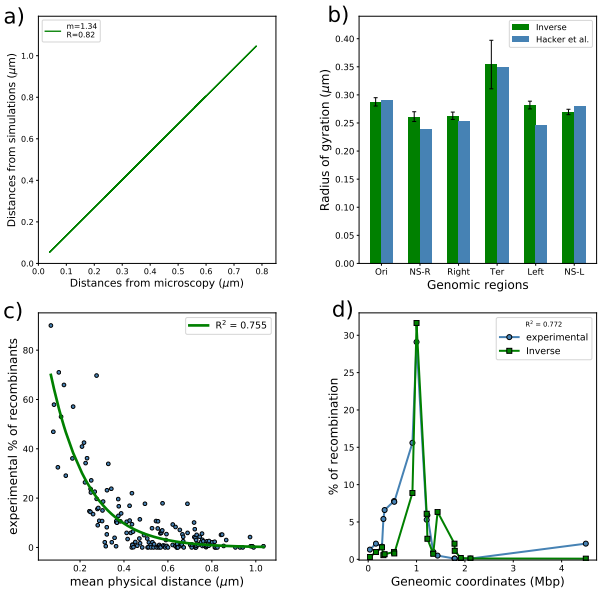

Figure S5: a) Comparison of distances measured via fluoroscence microscopy with distances obtained with simulations using inverse transfer function. **b)** Comparison of radii of gyration among domains with respect to Hacker *et. al*'s reported values for oriC@midcell in their plectonemic model[12]. **c)** Comparison between the recombination frequencies provided by *Valens et al. 2004* [13] vs. mean physical distance between recombination loci and the green line indicates the single exponential fit. **d)** A representative plot of recombination frequencies predicted by mean physical distance.
blue: experimental data. green: predicted by simulated data using inverse transfer function.

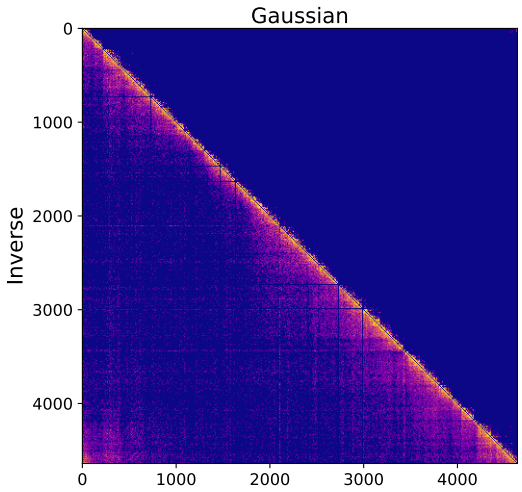

Figure S6: Comparison between the force constant matrices for Eqs. (**1**) and (S1) in the main text. The lower half of the plot is for Eq. (S1) while the upper half is for Eq. (**1**) in the main text.

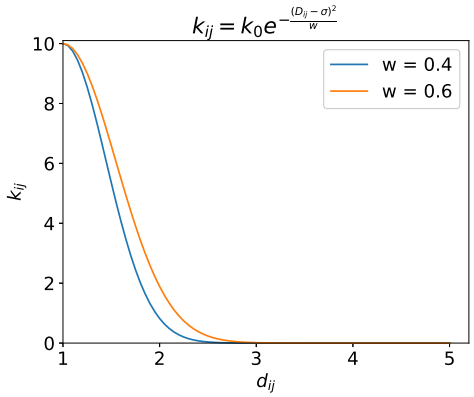

Figure S7: k_{ij} vs. D_{ij} (eqn (5)). σ=1.

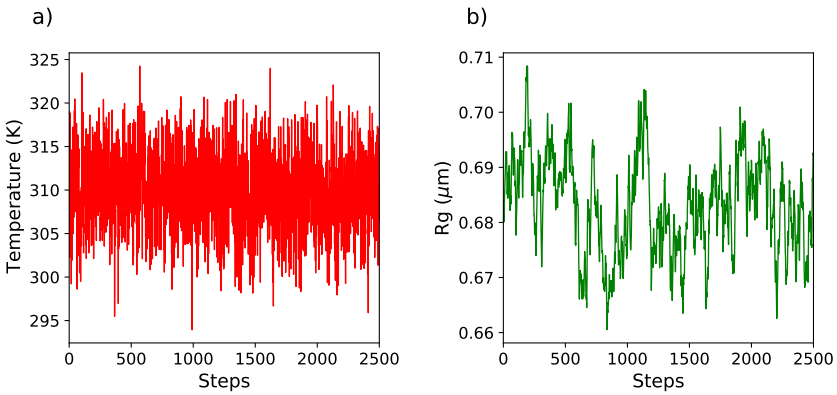

Figure S8: Validation that the system has reached equilibrium. **a)** Plot of temperature (K) vs. the steps. **b)** Plot of R_g vs. steps. The values reported here for one single trajectory.

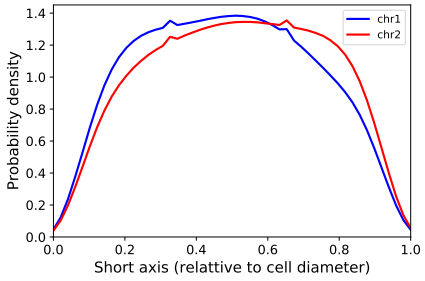

Figure S9: Linear density of chromosomes for G=3.6 along the short axis of the cell

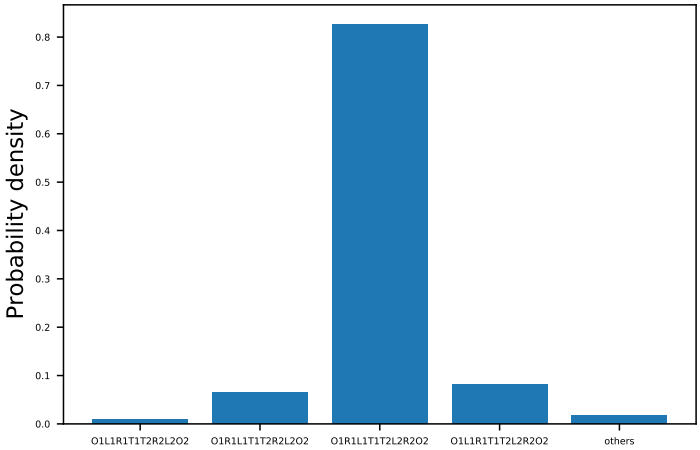

Figure S10: Probability histogram of orientation of the COG of the MDs for G=3.6

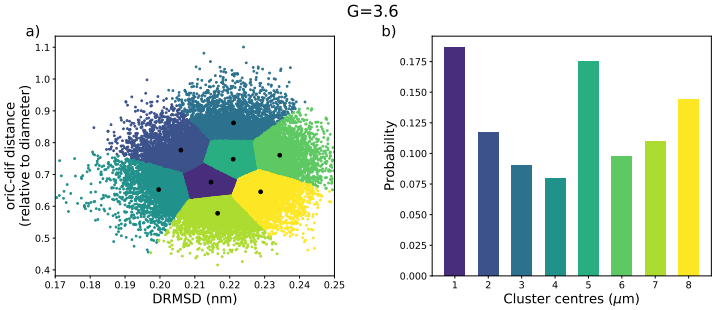

Figure S11: a) Conformation clustered using DRMSD and oriC-dif distance. The cluster centres have been represented as black dots. **b)** Probability distribution of clusters.

G=3.6

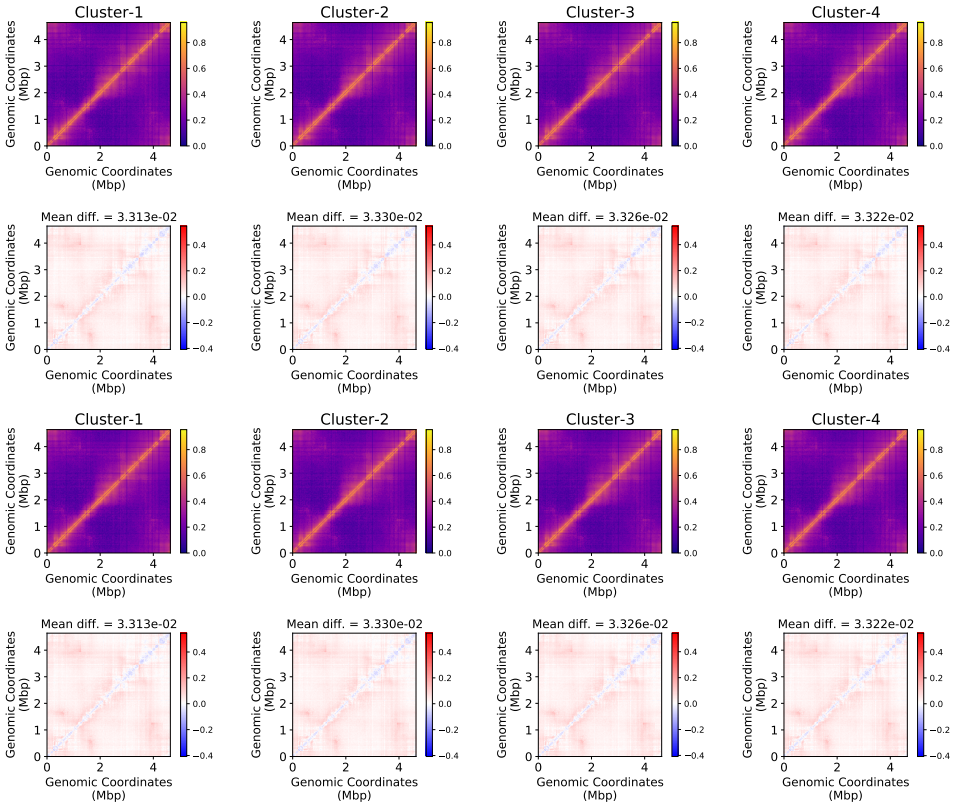

Figure S12: Simulated HiC matrices averaged over the conformations of each of their respective clusters have been plotted on the first and third rows. On the second and the fourth rows, the difference heatmap between the simulated matrices from the experimental matrix has been shown.

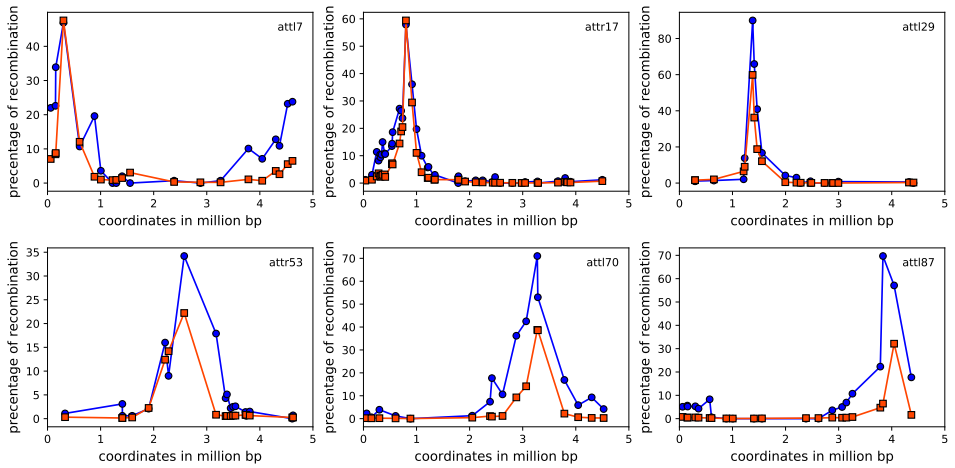

Figure S13: Predicted recombination frequency based on the exponential curve fitted in the figure **??** for 6 other loci (attl7, attr17, attl29, attr53, attl70, and attl87). Orange line indicates the fitted data and blue is experimentally observed data from *Valens et. al. (2004)*[13].

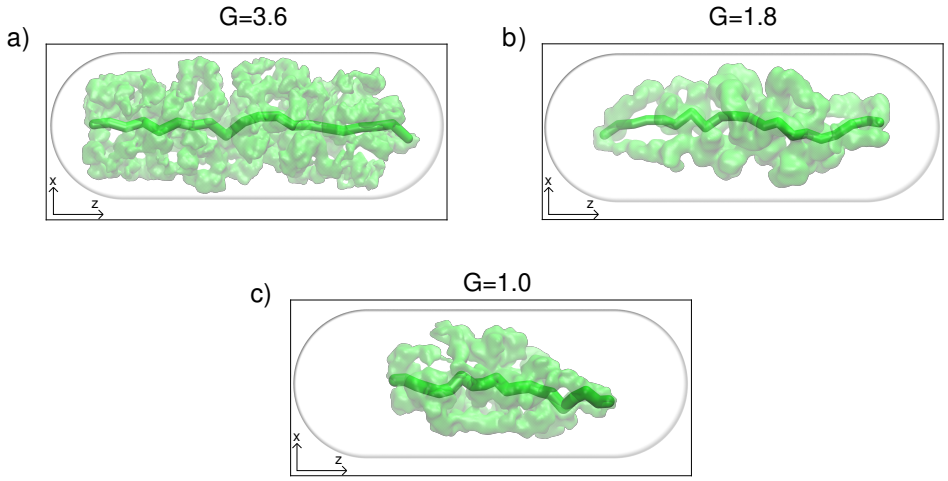

Figure S14: For each subfigure, the mean position of the beads of the particles present in a slice after z-slicing have been represented in green. The polymer has been represent as a transparent volume around it.

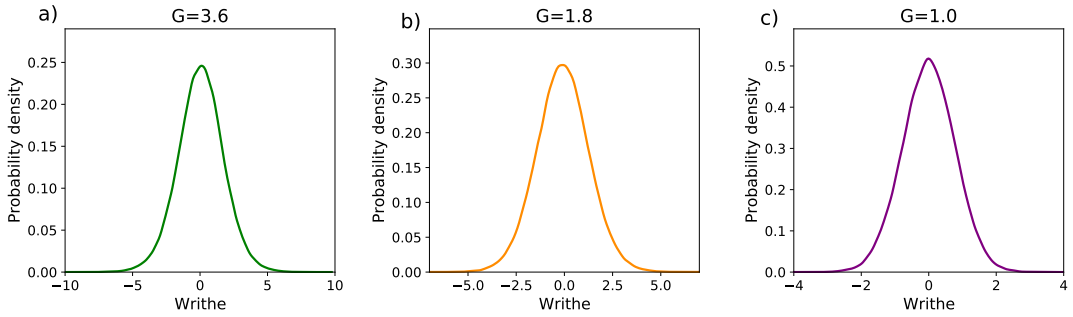

Figure S15: Distribution of writhe obtained by fitting each z-sliced frame to a polygon for G=3.6, 1.8 and 1.0.

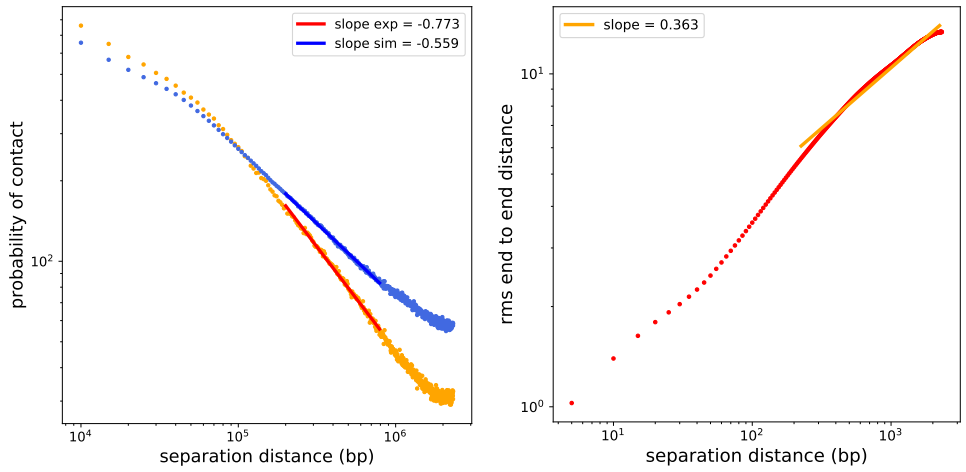

(a) Fractal globule plot

(b) Rms end-to-end distance plot

Figure S16: a) fractal globule plot for experimental and simulated contact probability matrix (orange: experimental, blue: simulated), **b)** mean of rms end-to-end distance of the genomic segments (in increasing length of 5000bp) vs. genomic distance (bp).

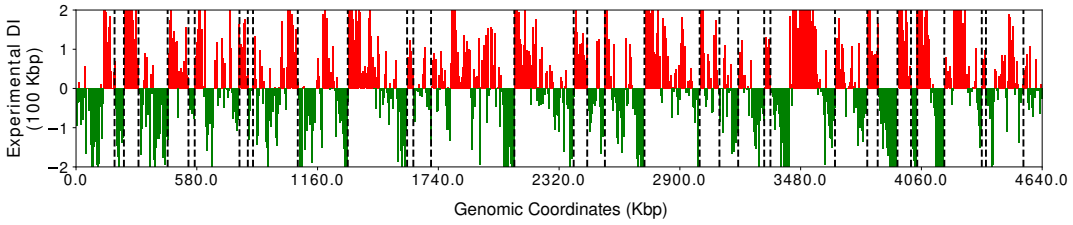

Figure S17: CID boundaries calculated using DI on the experimental contact probability matrix.

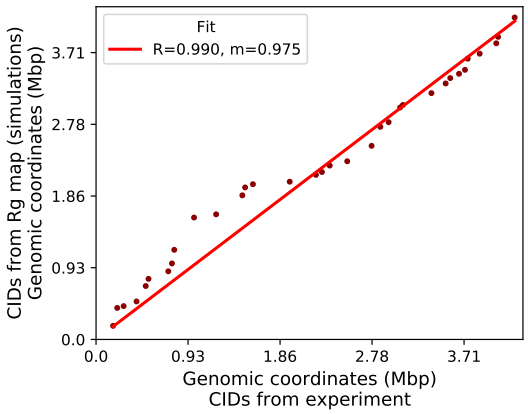

Figure S18: Correlation between CID boundaries detected by R_g map and DI

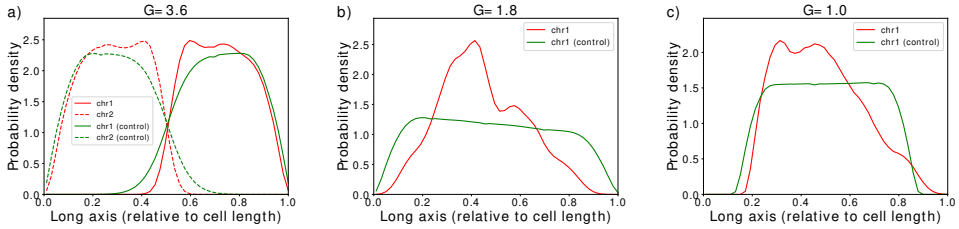

Figure S19: a) Comparison of linear densities of individual chromosomes between G=3.6 and its corresponding control scenario. **b)** Comparison of linear densities of chromosome for G=1.8 and its corresponding control scenario. **c)** Comparison of linear densities of chromosome for G=1.0 and its corresponding control scenario.

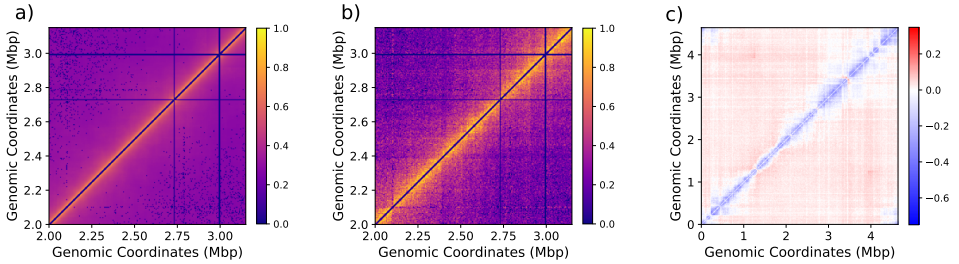

Figure S20: Comparison between matrices obtained from control simulations and experiments zoomed to a region near the diagonal. **a)** Contact probability matrix obtained from control simulations. **b)** Contact probability matrix obtained from experiments. **c)** Difference heatmap between matrices obtained from control simulations and experiments of the full matrix (without zoom).

References

[1] G Reshes, S Vanounou, I Fishov, and M Feingold. Timing the start of division in E. coli: a single-cell study. *Physical biology*, 5(4):046001, 2008.

[2] Saeed Saberi and Eldon Emberly. Chromosome driven spatial patterning of proteins in bacteria. *PLoS computational biology*, 6(11), 2010.

[3] HDPP Bremer, Patrick P Dennis, et al. Modulation of chemical composition and other parameters of the cell by growth rate. *Escherichia coli and Salmonella: cellular and molecular biology*, 2(2):1553–69, 1996.

[4] Virginia S Lioy, Axel Cournac, Martial Marbouty, Stéphane Duigou, Julien Mozziconacci, Olivier Espéli, Frédéric Boccard, and Romain Koszul. Multiscale structuring of the E. coli chromosome by nucleoid-associated and condensin proteins. *Cell*, 172(4):771–783, 2018.

[5] Annick Lesne, Julien Riposo, Paul Roger, Axel Cournac, and Julien Mozziconacci. 3D genome reconstruction from chromosomal contacts. *Nature methods*, 11(11):1141, 2014.

[6] Asli Yildirim and Michael Feig. High-resolution 3D models of caulobacter crescentus chromosome reveal genome structural variability and organization. *Nucleic acids research*, 46(8):3937–3952, 2018.

[7] Jagannath Mondal, Benjamin P Bratton, Yijie Li, Arun Yethiraj, and James C Weisshaar. Entropy-based mechanism of ribosome-nucleoid segregation in E. coli cells. *Biophysical journal*, 100(11):2605–2613, 2011.

[8] Somenath Bakshi, Albert Siryaporn, Mark Goulian, and James C Weisshaar. Superresolution imaging of ribosomes and RNA polymerase in live Escherichia coli cells. *Molecular microbiology*, 85(1):21–38, 2012.

[9] Lei Liu, Guang Shi, D. Thirumalai, and Changbong Hyeon. Chain organization of human interphase chromosome determines the spatiotemporal dynamics of chromatin loci. *PLOS Computational Biology*.

[10] William Humphrey, Andrew Dalke, and Klaus Schulten. VMD – Visual Molecular Dynamics. *Journal of Molecular Graphics*, 14:33–38, 1996.

[11] Olivier Espéli, Romain Mercier, and Frédéric Boccard. DNA dynamics vary according to macrodomain topography in the E. coli chromosome. *Molecular microbiology*, 68(6):1418–1427, 2008.

[12] William C Hacker, Shuxiang Li, and Adrian H Elcock. Features of genomic organization in a nucleotide-resolution molecular model of the Escherichia coli chromosome. *Nucleic acids research*, 45(13):7541–7554, 2017.

[13] Michèle Valens, Stéphanie Penaud, Michèle Rossignol, François Cornet, and Frédéric Boccard. Macrodomain organization of the Escherichia coli chromosome. *The EMBO journal*, 23(21):4330–4341, 2004.